PNAS
www.pnas.org

Supplementary Information for

Supraglacial lake drainage at a fast-flowing Greenlandic outlet glacier

Thomas R. Chudley, Poul Christoffersen, Samuel H. Doyle, Marion Bougamont, Charlotte M. Schoonman, Bryn Hubbard, Mike R. James

E-mail: trc33@cam.ac.uk or pc350@cam.ac.uk

This PDF file includes:

Supplementary text
Figs. S1 to S4
Table S1
Caption for Movie S1
References for SI reference citations

Other supplementary materials for this manuscript include the following:

Movie S1

www.pnas.org/cgi/doi/10.1073/pnas.1913685116

Supporting Information Text

Depth Correction of Photogrammetry-Derived Lake Bathymetry. Photogrammetry is known to underestimate the depth of water bodies observed from the air due to influence from refraction at the air-water interface (e.g. 1–6). Under idealised conditions, corrections can be determined precisely if the imaging geometry relative to the interface is known but, in the Photoscan software used here, the critical information on which photographs contribute to each individual point in the final model, is not available. Although estimates and simplifications can be used (7), through having repeat DEMs of the lake basin (i) prior to and (ii) following lake drainage, our study allowed us to infer an empirical correction factor on observed lake depth. This correction factor was derived as the slope of a linear regression performed between the apparent depth of the submerged regions and their 'true' position derived after lake drainage. Areas of <0.5 m apparent depth were eliminated prior to this regression as they often contained floating ice. We performed this regression across multiple comparisons between three DEMs of the highest water level (5^{th}, 6^{th}, and 7^{th} July) against the four DEMs of the lowest water level (12^{th}, 15^{th}, 24^{th}, 28^{th} July) in order to minimise the influence of vertical error and artefacting in individual DEMs. The average slope of the regression fit was 1.32, which was applied as the correction factor to all submerged regions of DEMs. We note that this value is within 1% of the refractive index of water – suggesting that, for our Photoscan-processed nadir image sets, a straightforward first-order refraction correction (e.g. 5) would suffice.

To produce a single time-averaged lake bathymetry for pressure-sensor depth-volume calculation, we median-averaged all the pre-drainage DEMs (5^{th}, 6^{th}, and 7^{th} July) before applying a 2 m gaussian filter in order to remove the impacts of floating lake ice, advecting crevasses, progressive ice surface ablation, and data artefacts present in individual DEMs.

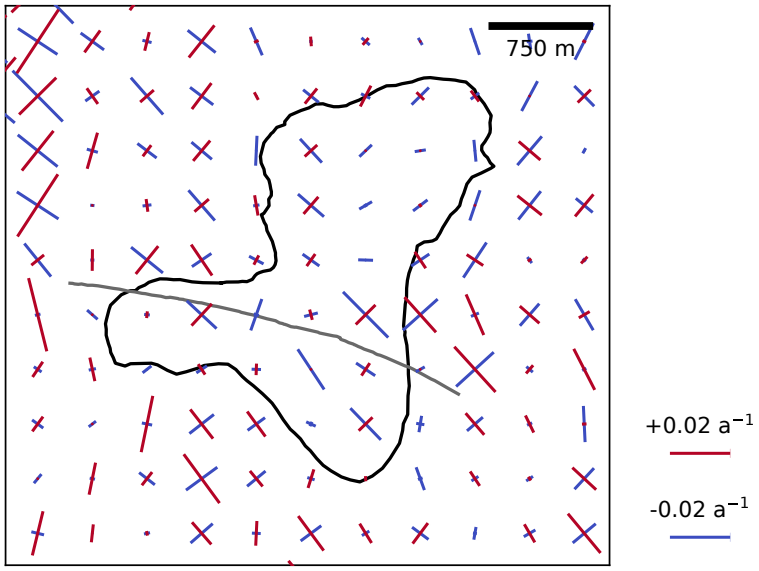

Fig. S1. Surface principal strain rates (red and blue lines) around Lake F derived from 2017 annual MEASUREs velocity data (8). Maximum lake extent (black) and fracture (grey) from (9). Note the order-of-magnitude difference in strain vector scale between this figure and figure 6.

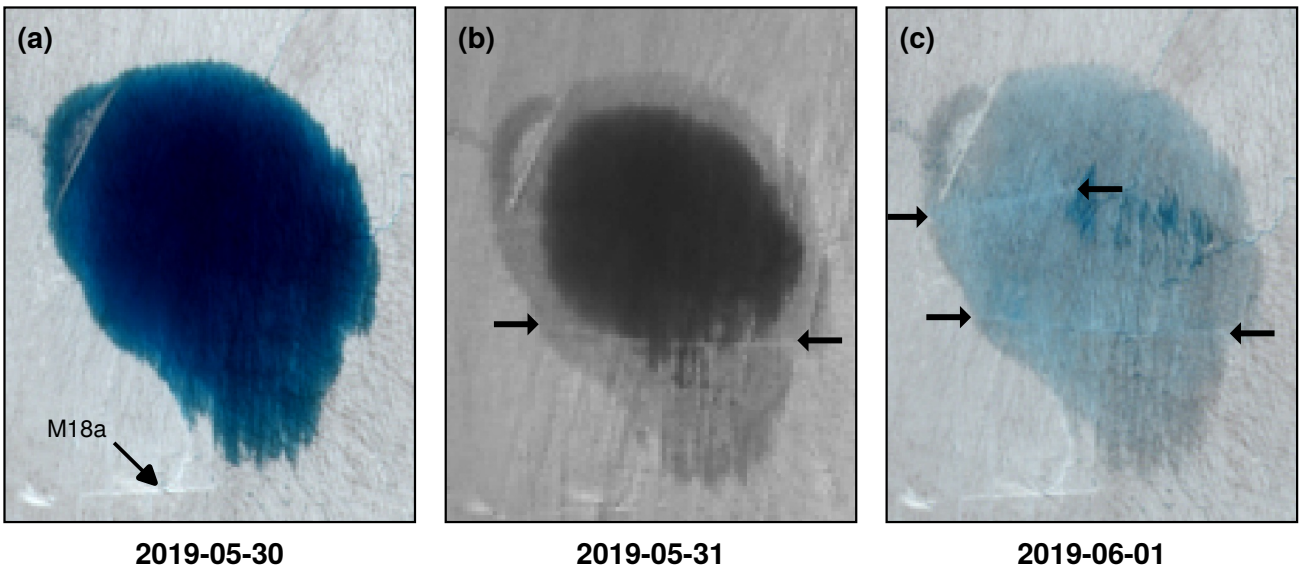

Fig. S2. The 2019 drainage of Lake 028 as captured by RGB Sentinel-2 (a, c) and panchromatic Landsat-8 OLI (b) imagery. Arrows identify the ends of drainage fractures.

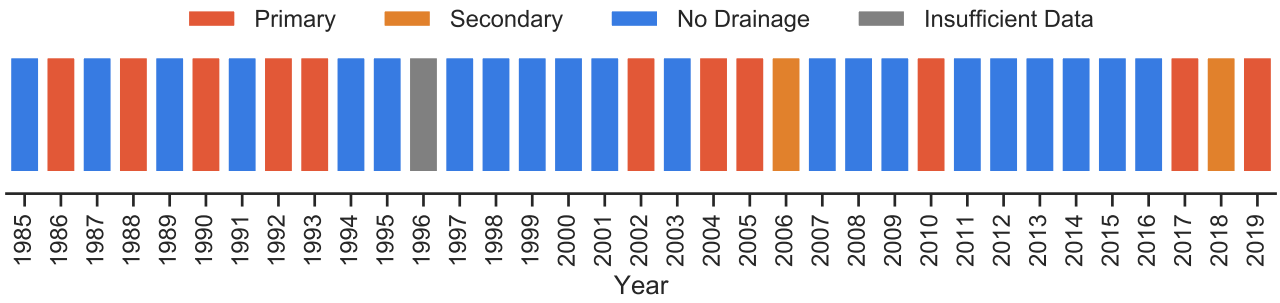

Fig. S3. Drainage history of Lake 028, as manually assessed from historical Landsat and Sentinel-2 data.

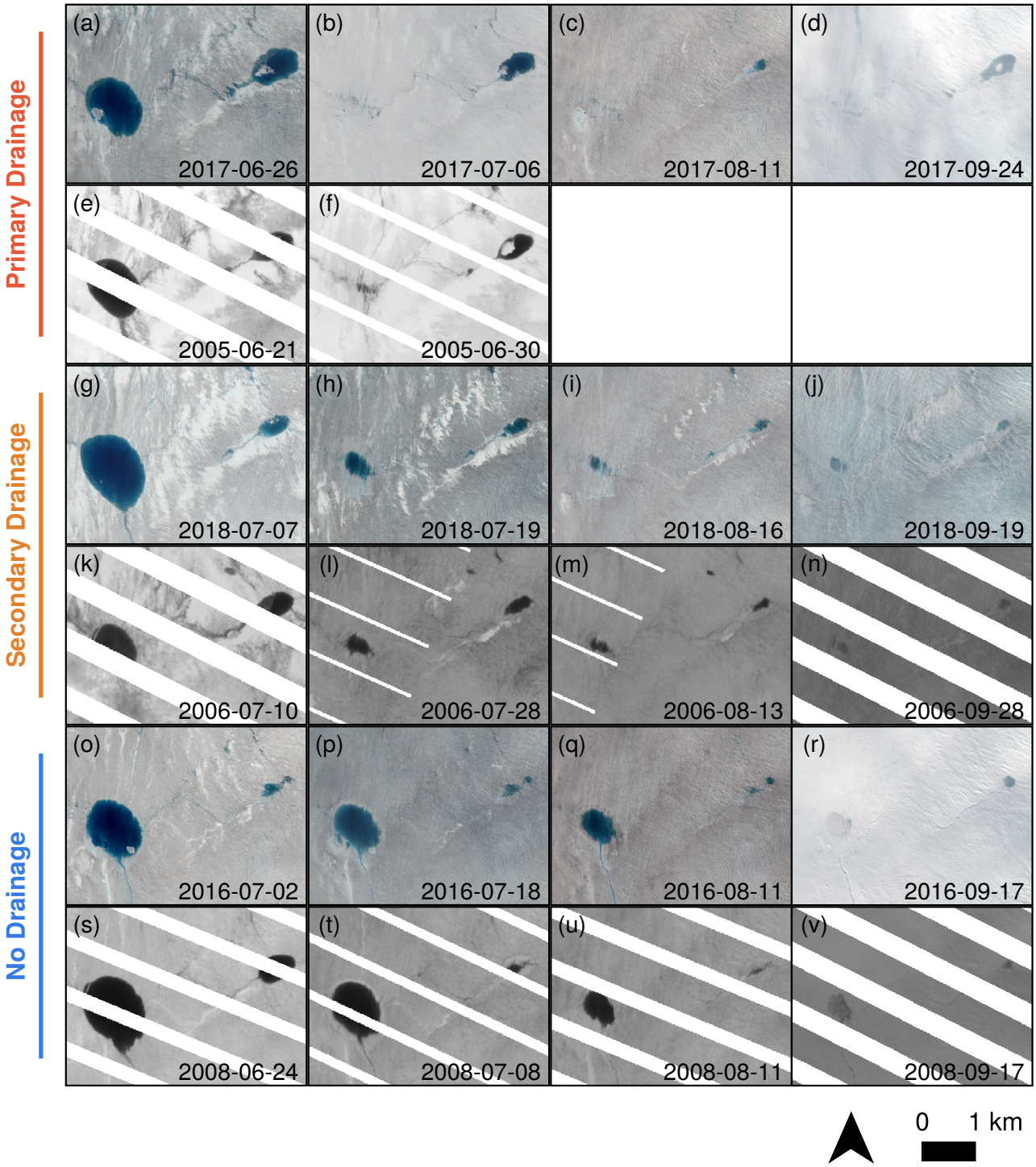

Fig. S4. Sentinel-2 false colour and Landsat 7 ETM+ (SLC-off) panchromatic imagery showing examples of the three modes of drainage of Lake 028 (left-hand lake in images) paired with Lake 031 (right-hand lake in images). (a–f) Type I 'primary' drainage occurring when Lake 028 had not drained the year before, showing the total loss of lake volume. (g–n) Type II 'secondary' drainage, occurring in years where type I drainage had occurred in the prior year, showing partial lake drainage and cut-off of outflow channel. (o–v) Examples of no drainage (NB the continuation of outflow channel, in contrast to reactivation drainage).

Table S1. Dates and time (UTC) of UAV flights used in this study. Times represent the midpoints of flights, rounded to the nearest five minutes. For further information on the 2017 flight, see (10)

Date	Time
2017-07-26	11:35
2018-07-05	02:00
2018-07-06	16:40
2018-07-07	12:45
2018-07-08	01:40
2018-07-08	15:15
2018-07-09	18:15
2018-07-12	15:25
2018-07-15	13:00
2018-07-18	12:00
2018-07-24	21:30
2018-07-28	12:50

Movie S1. Time lapse photography of the lake drainage taken every 10 seconds between 2018-07-07 21:21:10 and 2018-07-08 01:30:00. Displayed alongside is a zoomed-in and time-marked version of Figure 3 in the main text.

References

1. G Tewinkel, Water depths from aerial photographs. *Photogramm. Eng.* **29**, 1037–1042 (1963).
2. W Harris, M Umbach, Underwater mapping. *Photogramm. Eng.* **38**, 1037–1042 (1972).
3. J Fryer, Photogrammetry through shallow water. *Aust. J. Geod. Photogramm. Surv.* **38**, 25–38 (1983).
4. J Fryer, H Kniest, Errors in depth determination caused by waves in through-water photogrammetry. *The Photogramm. Rec.* **11**, 745–753 (1985).
5. R Westaway, S Lane, D Hicks, The development of an automated correction procedure for digital photogrammetry for the study of wide, shallow, gravel-bed rivers. *Earth Surf. Process. Landforms* **25**, 209–226 (2000).
6. C Mulsow, R Kenner, Y Bühler, A Stoffel, HG Maas, Subaquatic Digital Elevation Models from UAV-Imagery. *Int. Arch. Photogramm. Remote. Sens. & Spatial Inf. Sci.* **42** (2018).
7. JT Dietrich, Bathymetric structure-from-motion: extracting shallow stream bathymetry from multi-view stereo photogrammetry. *Earth Surf. Process. Landforms* **42**, 355–364 (2017).
8. I Joughin, BE Smith, IM Howat, T Scambos, T Moon, Greenland flow variability from ice-sheet-wide velocity mapping. *J. Glaciol.* **56**, 415–430 (2010).
9. SH Doyle, et al., Ice tectonic deformation during the rapid in situ drainage of a supraglacial lake on the Greenland Ice Sheet. *The Cryosphere* **7**, 129–140 (2013).
10. TR Chudley, P Christoffersen, SH Doyle, A Abellan, N Snooke, High-accuracy UAV photogrammetry of ice sheet dynamics with no ground control. *The Cryosphere* **13**, 955–968 (2019).